



Article

Dynamics Studies of Nitrogen Interstitial in GaN from Ab Initio Calculations

Huan He ¹, Wenbo Liu ¹, Pengbo Zhang ², Wenlong Liao ¹, Dayin Tong ¹, Lin Yang ³, Chaohui He ^{1,*}, Hang Zang ¹ and Hongxiang Zong ⁴

¹ School of Nuclear Science and Technology, Xi'an Jiaotong University, Xi'an 710049, China; hehuan0422@stu.xjtu.edu.cn (H.H.); liuwenbo@xjtu.edu.cn (W.L.); lw1551528661@stu.xjtu.edu.cn (W.L.); tdy8008208820@stu.xjtu.edu.cn (D.T.); zanghang@xjtu.edu.cn (H.Z.)

² School of Physics, Dalian Maritime University, Dalian 116026, China; zhangpb@dlmu.edu.cn

³ Department of Chemistry, University of Manchester, Manchester M13 9PR, UK; lin.yang-10@postgrad.manchester.ac.uk

⁴ State Key Laboratory for Mechanical Behavior of Materials, Xi'an Jiaotong University, Xi'an 710049, China; zonghust@mail.xjtu.edu.cn

* Correspondence: hechaohui@xjtu.edu.cn

Received: 14 July 2020; Accepted: 13 August 2020; Published: 17 August 2020



Abstract: Understanding the properties of defects is crucial to design higher performance semiconductor materials because they influence the electronic and optical properties significantly. Using ab initio calculations, the dynamics properties of nitrogen interstitial in GaN material, including the configuration, migration, and interaction with vacancy were systematically investigated in the present work. By introducing different sites of foreign nitrogen atom, the most stable configuration of nitrogen interstitial was calculated to show a threefold symmetry in each layer and different charge states were characterized, respectively. In the researches of migration, two migration paths, in-plane and out-of-plane, were considered. With regards to the in-plane migration, an intermediated rotation process was observed first time. Due to this rotation behavior, two different barriers were demonstrated to reveal that the migration is an anisotropic behavior. Additionally, charged nitrogen Frenkel pair was found to be a relatively stable defect complex and its well separation distance was about 3.9 Å. Part of our results are in good agreement with the experimental results, and our work provides underlying insights of the identification and dynamics of nitrogen interstitial in GaN material. This study of defects in GaN material is useful to establish a more complete theory and improve the performance of GaN-based devices.

Keywords: ab initio calculation; nitrogen interstitial; migration; rotation; Frenkel pair

1. Introduction

Gallium nitride (GaN) with a wide-gap (~3.4 eV) is an excellent semiconductor material. Nowadays, it has been widely used in visible–UV light emitting devices (LEDs) [1], laser diodes (LDs), 5G communications, and high power/frequency transistors [2,3] because of its outstanding properties, such as high electron mobility and high breakdown voltage. Additionally, the high radiation tolerance [4,5] of GaN makes it a promising material for the application in satellites [6]. However, in the process of GaN growth, the large lattice mismatch of GaN with its substrate (silicon carbide (SiC) or sapphire) is inevitable. In addition, there are varieties of defects appearing in the whole fabrication process, including native point defects and impurities, such as C, O, H, as well as dislocations [7,8]. Therefore, it is still a big challenge to improve the performance of GaN-based devices.

The influence of defects in GaN material has been studied by experimental or theoretical work for years. With deep levels transient spectroscopy (DLTS), Kanegae et.al [9] observed that E_3 ($E_c - 0.60$ eV)

and H_1 ($E_v + 0.87$ eV) are dominating traps in n-type GaN, and they attributed H_1 trap to the gallium vacancy or C related defects. Sunay et.al [10] applied electron paramagnetic resonance (EPR) to find that the hole is around the Mg acceptor. In addition, by using positron annihilation spectroscopy (PAS), EPR, and density functional theory (DFT), Bardeleben et.al [11] found that the isolated N interstitial is unstable and prefers to form a split interstitial configuration, which is located at $E_c - 1.0$ eV. However, experimental devices have limitations, i.e., DLTS can only obtain the energy level but not the specific type of defect.

Therefore, it leaves much room for theoretical simulation works, which can help us understand these defects from the atomic level. As an important complementarity, theoretical simulation is another efficient approach to understanding the property of defects. Among the theoretical work on GaN, varieties of studies [12–17] were put forward to obtain the transition levels related to the defects. They eventually concluded that N_i can occupy five charge states within the band gap. However, in some cases, such as under the doping process or radiation environment, the defects may move among the material and interact with other defects, instead of keeping as static ones. In contrast with abundant of calculations of static properties, less is known about the dynamics studies of defects [18,19], especially the interaction of defects.

In order to achieve a better understanding of defects in GaN material, in this paper, we performed ab initio calculations that focus on the nitrogen interstitial (N_i). First, the most stable configurations of different charge states were calculated. Then, the migration of it was studied and a rotation process, which was not reported in previous researches, was included. Finally, its interaction with vacancy (V_N) was systematically investigated.

2. Methods

Density functional theory calculations were performed with the Vienna Ab initio Simulation Package (VASP) 5.4.4 [20] code using pseudopotentials generated with the projector augmented wave (PAW) approach. The exchange-correlation function was treated with the generalized gradient approximation (GGA) using the parameterization by Perdew, Burke, and Ernzerhof (PBE) [21,22]. The valence electron configurations of $2s^2 2p^3$ for N and $3d^{10} 4s^2 4p^1$ for Ga were considered. The supercell method was applied with the periodic boundary conditions. Specifically, $4 \times 4 \times 2$ supercell with 128 atoms was large enough to use in our simulations. The gamma k-point mesh was set to $2 \times 2 \times 2$, and the cutoff energy was set as 500 eV. The convergence of force was less than 0.01 eV/Å for all the computations, while the criterion of energy was minimized to a value of 10^{-5} eV. Climbing image nudged elastic band (CI-NEB) method [23] was used to investigate the migration processes and their corresponding possible minimum energy path, as well as the recombination process. Furthermore, in order to obtain an accurate transition state faster, DIMER method [24] was applied sometimes within CI-NEB method. The criterions of energy and force applied in these two methods were the same as the values in the optimization of structures.

The model of GaN crystal was based on the Material Project database [25], and after structure optimization, lattice parameter was eventually optimized to $a = 3.219$ Å and $c/a = 1.632$, which matched well with the previous experiments [26]. As shown in Figure 1a, every N atom was bonded with four Ga atoms and the bond length is 1.97 Å. Additionally, there are two distinct N layers in a perfect GaN crystal, named “A” and “B” layer, characterized by the orientation of N atom with the nearest Ga atoms. As shown in Figure 1b, the orientations of A layer were opposite to those of B layer.

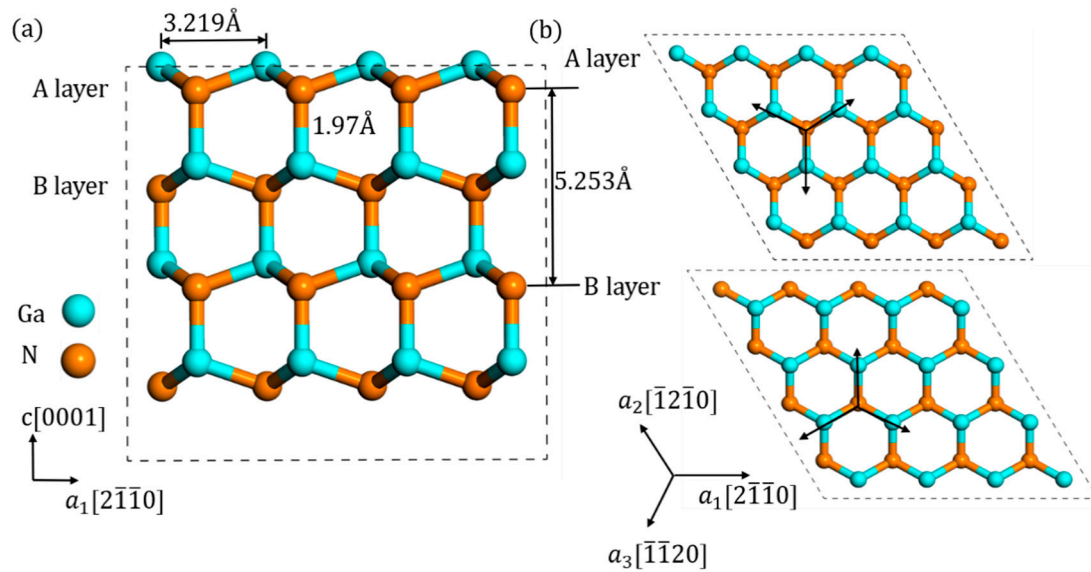


Figure 1. Different view of the structure of wurtzite GaN material: (a) side view and (b) top view of A layer and B layer.

The formation energy of a charged N_i is described as follows Equation (1) [27]:

$$E_f[N_i^q] = E_{\text{tot}}[N_i^q] - E_{\text{tot}}[\text{bulk}] - \mu_N + q(E_F + E_g) + E_{\text{corr}}^q \quad (1)$$

where $E_{\text{tot}}[N_i^q]$ is the total energy of supercell with charged defects, while $E_{\text{tot}}[\text{bulk}]$ is the total energy of system without defects. μ_N is the chemical potential of the N element. Additionally, E_F is the Fermi level, which is regarded as a variable, ranging from 0 to the band gap value E_g . Additionally, the last term is a correction term of the supercell system.

3. Results

3.1. Configurations of N_i

With regards to typical interstitials in hexagonal close packing (hcp) type materials, two types of high symmetry sites are the most common ones: the tetrahedral (T-site) and octahedral (O-site) sites. The T-site has four nearest neighbors and the O-site has six nearest neighbors. Therefore, it was first required to determine the most stable configuration of N_i . Tens of (more than 50) possible sites were carried out assuming that N_i could locate in any possible space in the crystal. The results revealed that wherever the initial N_i is, even the O or T sites, it always prefers a split interstitial configuration. This configuration is a N-N dimer tilted bond as presented in Figure 2, and the calculated formation energy of the neutral state is 4.67 eV. These findings correspond to the previous researches [12,14,17] well. Furthermore, some new specific characteristics of these N_i were concluded, and they could be directly applied in later simulations or experiments.

Because of the high symmetry of wurtzite structure, as shown in Figure 1, the tilted N_i should be sixfold symmetry. However, due to the different orientations of N atom with its nearest Ga atoms, the tilted N_i presents a threefold symmetry in each layer, respectively, not a true sixfold symmetry. These threefold symmetry configurations can transform to each other by rotating [0001] axis by multiples of 120° . The example of three configurations on A layer, named “A₁,” “A₂,” and “A₃” is shown in Figure 2, and the following discussions are mainly based on this A₁ configuration. Note that the foreign atom can become either atom in this dimer bond. Due to the tilting characteristic, its direction’s projection on the c-plane is the same as that between the origin N atom with the nearest Ga atom, which is $[1-10c]$ (parameter c is about 1.75). Additionally, its bond length is measured about

1.35 Å. This N-N bond length is a little larger than N₂ gas molecule (1.11 Å) and much less than normal Ga-N bond length (1.97 Å), which indicates that it may be a relatively stable bond. The schematics of configurations on B layer are included in Figures A1–A3 in Appendix A.

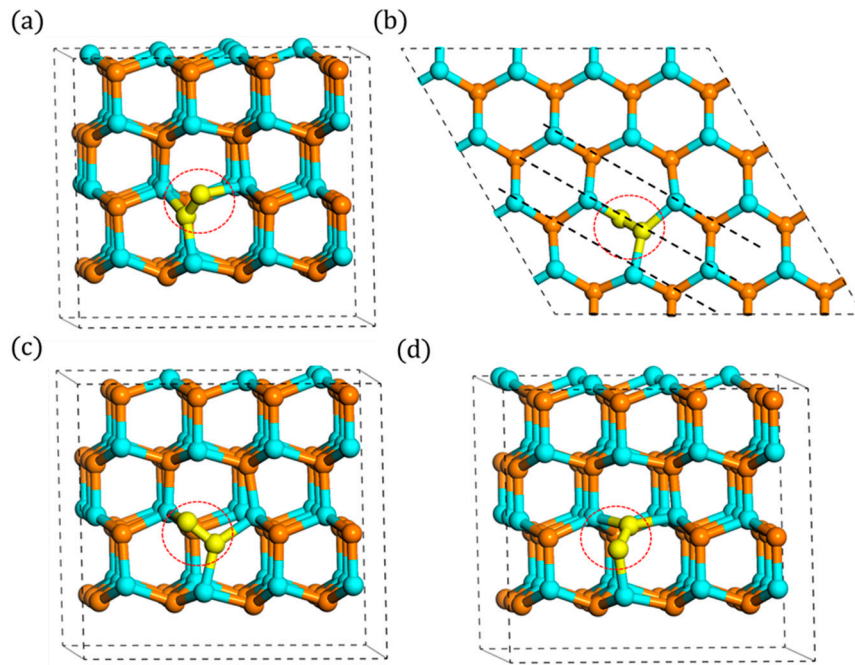


Figure 2. Configurations of split interstitial: (a) side view of A₁, (b) top view of A₁, (c) side view of A₂, and (d) side view of A₃ (N_i atoms are denoted by yellow spheres, the same below).

As discussed in other studies [12,13,18,27], N_i always occupies five charge states (−1 to 3) within the band gap. Therefore, the charge state of −1 to 3 was considered in our research. With regards to different charge states, the bond length of N_i changes significantly, from 1.44 to 1.15 Å. However, the directions are like the neutral ones. The differences between them mainly reflect on the parameter *c*, and the corresponding results are listed in Table 1. Comparing the values in Table 1, the bond length of N_i was found to increase as the charge state decreases, indicating that positive charge states may provide a more attractive force than negative charge states. On the other hand, our calculated bond length is consistent well with previous work [18,27].

Table 1. Bond length and parameter *c* of different charge states of N_i.

Charge State	<i>d</i> _{N-N} (Å)			Parameter <i>c</i>
	This Work	Other Work	Other Work (%)	
3	1.15	1.12 ^a 1.11 ^b	2.61 ^a 3.48 ^b	1.50
2	1.20	1.18 ^a	1.67 ^a	1.51
1	1.27	1.25 ^a	1.57 ^a	1.55
0	1.35	1.34 ^a	0.74 ^a	1.75
−1	1.44	1.45 ^a 1.41 ^b	0.69 ^a 2.08 ^b	2.27

^a Reference [19]; ^b Reference [17].

3.2. Migration of N_i

Because of the lower formation energy among the simple point defects, N_i is one of the most common native defects in the GaN material. Therefore, its migration behavior influences the properties of material significantly. As shown in Figure 3a, there are two possible migration paths, in-plane and out-of-plane. Only the first nearest neighbor (1NN) atoms were considered here. With regards to six

nearest atoms in-plane, determined by the orientation of N_i , the migration could be divided into three categories, A, B, and C site, as shown in Figure 3b. Since C site is symmetrical with A site, only A and B site was taken into consideration. Furthermore, the upward one (N_{up}) in N_i was regarded as the atom to migrate.

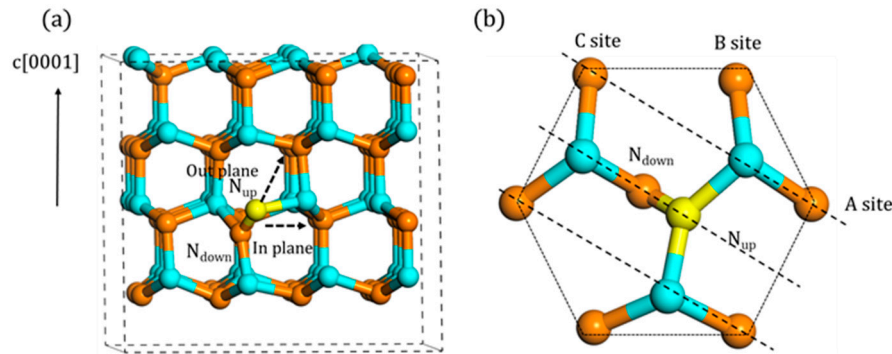


Figure 3. The migration mechanism of A_1 type N_i atom (the yellow atom is migrated N atom, the same as below): (a) two possible paths and (b) the top view of the in-plane migration.

3.2.1. In-Plane Migration

With regards to the A site, two different migration mechanisms of N_i are found. The first one is a direct migration, the N_{up} atom first breaks the bond of interstitial and then directly migrates to the A site, forming a new type N_i . The corresponding migration process is shown in Figure 4a. Note that the initial state (a-1) is different from the final state (a-3), which is another type of orientation in this layer. Furthermore, its related energy barrier is shown in Figure 4b, and the migration barrier is 2.34 eV, which is consistent well with previous studies, i.e., 2.33 eV [14] and 2.4 eV [17,18].

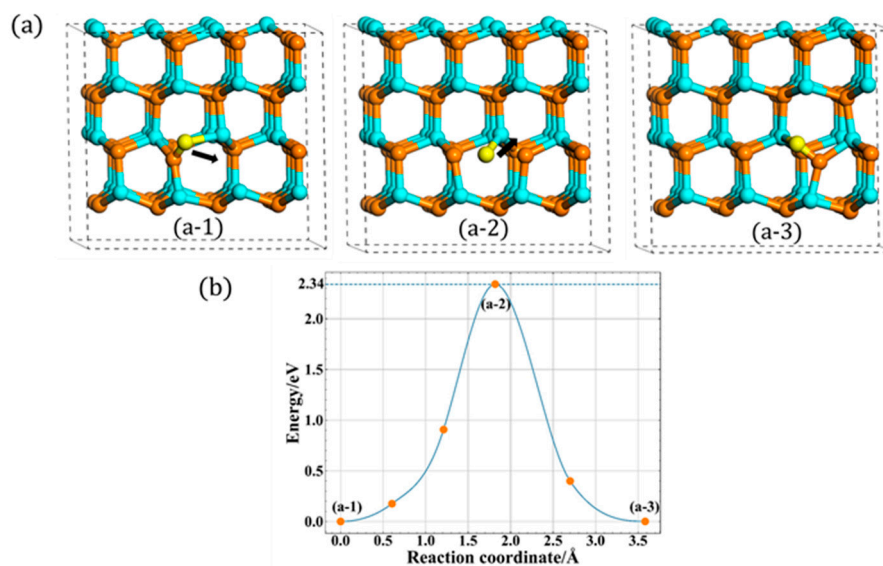


Figure 4. The direct in-plane migration for A site: (a) the process of direct migration. (b) The corresponding energy barrier (the solid dots are interpolated points and the solid line show the energy path obtained from CI-NEB methods).

Compared with the previous studies [16,17] of migration, a new indirect migration was observed in our study, as shown in Figure 5a. In this indirect process, the N atom's migration behavior is a little different while a rotation behavior occurs first during the whole migration process. First, it rotates around the c-plane with relatively low energy barrier, about 0.35 eV. During the rotation process,

the bond length increases first and then decreases to the stable configuration, which is another type of configuration (A_2) in this layer. After the rotation process, the N atom starts to move and then migrates to A site. Compared with the direct migration, there are two different points. First, the final state (a-4) is the same as the initial state (a-1) before rotation. Second, the migrated atom transfers finally to the lower site after the whole migration. The whole process is presented in Figure 5b, and the migration barrier is 2.43 eV, slightly larger than the first type of migration path. And the animations of these two migration are included in Figures S1 and S2 in Supplementary Materials.

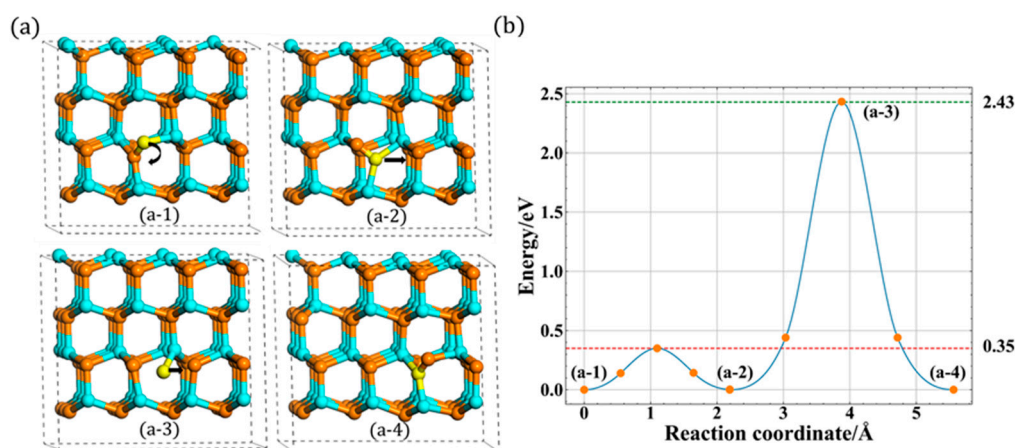


Figure 5. The indirect in-plane migration for A site: (a) the process of indirect migration and (b) the corresponding energy barrier.

However, this little difference (2.34 vs. 2.43 eV) is not actually influenced by the rotation behavior, because these different migration barriers were also observed when the N atom migrates to B site with two different indirect migrations. With regards to B site, the N atom cannot migrate directly like the case of the A site, since B site is far away from the A_1 type's orientation. Therefore, it must rotate first to A_2 or A_3 type, and then, it migrates directly to B site. When it starts to migrate from A_2 type, the migration barrier is 2.43 eV, the same as the indirect migration to A site. However, when it rotates first to A_3 type, this process only needs 2.34 eV, which is equivalent to the direct migration. This phenomenon, as shown in Figure 6, illustrates that the different migration barriers (2.43 vs. 2.34 eV) are not influenced by the rotation process. In addition to this, it also can be seen that when the N atom presents downward migration, the migration barrier is 2.43 eV, whereas when the N atom migrates upward, the value changes to 2.34 eV.

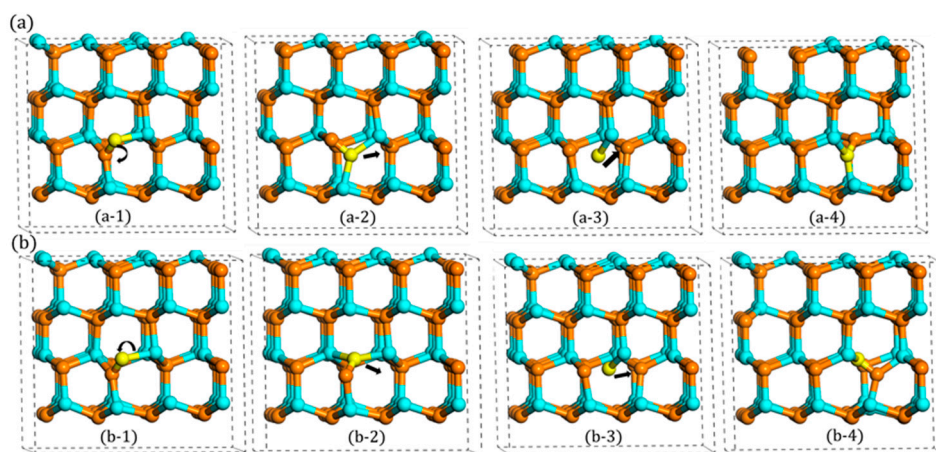


Figure 6. Two rotation-migration mechanisms to B site: (a) A_1 rotates to A_2 and (b) A_1 rotates to A_3 .

In summary, the in-plane migrations actually have two paths, upward and downward ones. Additionally, they can transform to each other by the rotation behavior. The schematic is shown in Figure 7. Additionally, as shown in Table 2, under high charge states, the difference of migration barriers is a little large. Therefore, by introducing the consideration of rotation behavior of N interstitial, it is found that the in-plane migration of N atoms is an anisotropic behavior, which is different from the conclusions of previous studies [16,17].

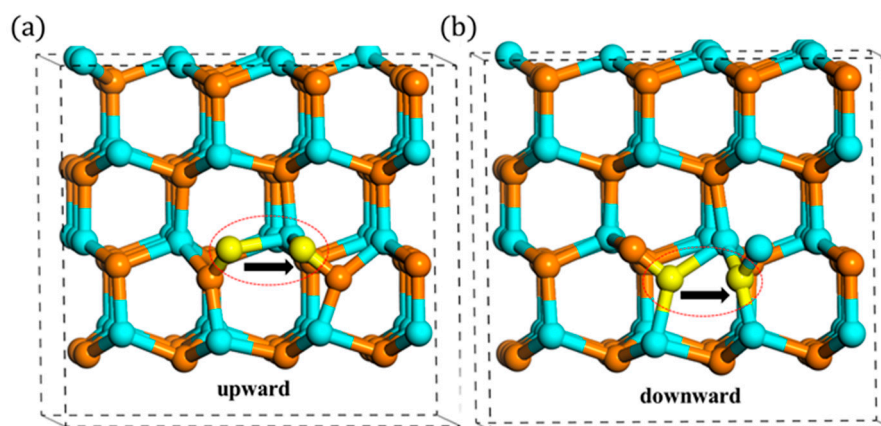


Figure 7. (a) Upward and (b) downward migration (the left yellow atom migrates to the right yellow atom).

3.2.2. Out-of-Plane Migration

With regards to out-of-plane migration of N_i , the results are like previous work [16,17] and show that it could be a direct migration as discussed above. All of the detailed values are also listed in Table 2.

Table 2. Rotation and migration barriers for different charge states of N_i .

Charge State	Rotation Barrier/eV	In/eV(upward/downward)	Out/eV	In/eV	Out/eV
−1	0.33	1.80/1.80	1.87	1.9 ^a , 1.6 ^b	1.9 ^a , 1.6 ^b
0	0.35	2.34/2.43	2.40	2.4 ^a , 2.4 ^b , 2.33 ^c	2.4 ^a , 2.4 ^b
1	0.27	2.48/2.52	2.18	2.2 ^a , 2.1 ^b	2.1 ^a , 2.1 ^b
2	0.24	1.98/2.08	2.13	2.1 ^a , 2.5 ^b	2.2 ^a , 2.5 ^b
3	0.23	1.57/1.26	2.13	2.1 ^a , 1.4 ^b	1.7 ^a , 1.4 ^b

^a Reference [19]; ^b Reference [18]; ^c Reference [14].

The data in Table 2 indicates that the rotation and migration barriers vary in the different charge states and part of our results are consistent well with previous work [14,18,19]. The results show that the differences between the upward and downward paths in plane are due to the rotation barrier. Additionally, the migration barriers of in-plane and out-of-plane are also different. However, previous studies about migration of N_i did not observe the rotation behavior and concluded that it is an isotropic behavior with the same energy barriers from the in-plane to out-of-plane [18]. In our detailed researches, although the rotation barrier of 0.04–0.31 eV is very small compared with migration barriers of about 2 eV, its existence shows that the migration of N_i is not the same, especially in the migration mechanisms. Additionally, under room temperature, according to the Arrhenius equation, the difference of 0.1 eV may cause several orders of magnitude difference of gigahertz, which cannot be neglected in the application of high frequency devices [28,29]. Due to this little barrier, the migration process of N_i can present different possibilities, not merely a direct migration, and the rotation behavior provides a new perspective of the migration of N_i by the theoretical work. Therefore, the migration barrier is concluded to be an anisotropic behavior by the calculations about different migration barriers.

3.3. Stability of N_i-V_N Complex

Frenkel pair, as a common type of defect pair in material, plays an important role in the material property, especially under irradiation or ion modification. However, there are a few studies about this type of defect pair in GaN material, especially the theoretical work. Furthermore, the formation energy of neutral one is 6.82 eV, a little larger than the value of the isolated one, meaning that N Frenkel pair is easier to appear. Therefore, the stability of N Frenkel pair (N_i-V_N) was investigated here and the charge states of 0 to +3 were considered due to the possible charge states of isolated defects. Since N_i is a tilted configuration, a range of initial distances (d_{FP-id}) of N_i-V_N were considered for different charge states. Additionally, the separation distance (d_{FP-sd}) is defined as the nearest distance of the final N_i-V_N .

As expected, due to the large bond length of N_i , the recombination (annihilation of interstitial and vacancy, $N_i + V_N \rightarrow N_N$) is not observed for variety of N_i-V_N , except the neutral one with the nearest d_{FP-id} (2.75 Å) (in the following discussions, this specific condition is not considered). This phenomenon indicates that N_i is a type of relatively stable defect since it cannot nearly recombine spontaneously. In addition, consequently, N_i and V_N remain to locate their site and the N_i bond does not break itself. The bond lengths of N_i in N_i-V_N are illustrated in Table 3. Compared with the values in Table 1, the bond length of N_i in $(N_i-V_N)^q$ ($0 \leq q \leq 3$) is found to be almost equal to it of $(N_i)^{q-1}$. Accordingly, $(N_i-V_N)^q$ is assumed to consist of $(N_i)^{q-1}$ and $(V_N)^{+1}$. In order to verify this point more accurately, a more detailed charge analysis of these defects, containing N_i-V_N , isolated N_i and V_N , is required to be carried out.

Table 3. Bond lengths of N_i in the nearest N_i-V_N for different charge states.

Defect Type	Charge State	Bond Length/Å
N_i-V_N	+3	1.21
	+2	1.26
	+1	1.34
	0	1.44

Bader charge analysis [30,31] is used to investigate the charge transfer between atoms quantitatively. With regards to the perfect material, each N atom gains 1.54|e| from its four nearest Ga atoms, vice versa. However, when the system contains N_i defects, this value changes a lot. For the neutral one, the charges of two N_i atoms are identical to become 0.87|e|, and other Ga and N atoms in this system almost do not change. This phenomenon shows that due to the introduction of N_i , the charge of one original N atom decreases and this decrement mainly transfers to the foreign N atom. Since the charges of two N_i atoms are identical, their average values are adopted in the comparison. As for V_N , due to its special property without atoms, the average charges of the four nearest Ga atoms are considered instead. The comparisons between them are shown in Table 4.

Table 4. Bader charges of N_i , V_N in the nearest N_i-V_N and isolated N_i , V_N .

Defect Type	Charge State	N_i-V_N (N_i/V_N)	Isolated One (N_i/V_N)
Bader Charge(e)	3	0.51/1.23	0.21/1.43
	2	0.67/1.21	0.44/1.28
	1	0.84/1.19	0.66/1.21
	0	1.04/1.22	0.87/1.15
	−1	—	1.05/1.07

Compared with the Bader charge of N_i-V_N and isolated defects, the Bader charges of N_i and V_N in $(N_i-V_N)^q$ are consistent well with the values of isolated ones, e.g., $(N_i-V_N)^{+2}$ (0.67/1.21 |e|), $(N_i)^{+1}$ (0.66 |e|) and $(V_N)^{+1}$ (1.21 |e|). This accurate comparison suggests that for the N_i-V_N in the q charge state, this configuration could be associated with the reaction of $(N_i)^{q-1}$ and $(V_N)^{+1}$, namely, $(N_i-V_N)^q \rightarrow (N_i)^{q-1} + (V_N)^{+1}$. The charge state of V_N always remains the constant value of +1 in N_i-V_N pair. This similar relationship is also found in Si material [32], however, in their studies, they observed that

Si interstitial is the defect that remains as constant charge. Additionally, this phenomenon may explain that why only the neutral nearest N_i-V_N recombine spontaneously, since the neutral N_i-V_N is consist of $(N_i)^{-1}$ and $(V_N)^{+1}$ and they are exactly opposite charge.

Therefore, as mentioned above, the binding energy, which is often used to evaluated the stability of defect complex, is defined as Equation (2):

$$E_b = (E_{(N_i-V_N)^q} + E_{\text{perfect}}) - (E_{(N_i)^{q-1}} + E_{(V_N)^{+1}}) \quad (2)$$

Note that $E_b < 0$ means attraction and $E_b > 0$ means repulsion for this definition. By introducing different d_{FP-id} of N_i-V_N , the binding energies with different d_{FP-sd} were obtained in Figure 8. From this figure, the binding energy of N_i-V_N was observed to be influenced by the d_{FP-sd} . As the d_{FP-sd} increases, the binding energy increases first and then stays at about 0 eV from 3.9 Å, which indicates that the well-separated distance of N_i-V_N is 3.9 Å.

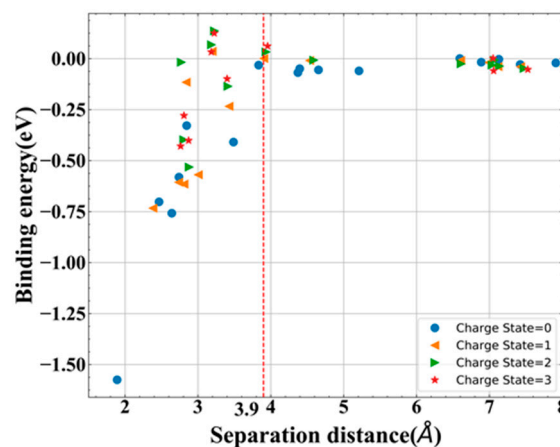


Figure 8. Binding energy of different charge states of N_i-V_N as a function of d_{FP-sd} .

Besides that, with the help of NEB method, the recombination barrier of the well-separated neutral N_i-V_N ($d_{FP-sd} = 3.9$ Å) is found to be 2.1 eV, which also verifies that this distance is a truly well separation distance from another perspective. It is worth noting that this recombination barrier is a little less than the migration barrier. Furthermore, the nearest neutral ($d_{FP-sd} = 1.89$ Å) one is also calculated to be 0.15 eV. Such small barrier value indicates that this distance of N_i-V_N is a metastable defect complex with strong binding, and it is easier to annihilate under ambient temperature.

3.4. Comparisons with the Experiments

A previous EPR experimental study [11] reported that N_i starts to anneal at 673 K during the first annealing stage, and this process of annealing may relate to the migration process. Additionally, the experiments also showed that this N_i locates at the Fermi level 1 eV below the conduction band minimum, indicating that it most likely corresponds to -1 charged state. Therefore, in order to verify our computation results, the reported experimental results were implemented to compare. According to the previous studies [33,34] of the correlation between activation energy and temperature, Arrhenius law was applied to the activation energy in most of cases. Thus, based on the Equation (3) of Arrhenius law, the activation energy, namely, the migration energy, is given by:

$$k = Ae^{-\frac{E_a}{k_B T}} \quad (3)$$

where k is the rate constant, which is always regarded as 1 Hz [34]. Additionally, the pre-exponential factor A is always represented by the material's Debye frequency of 13 THz [35]. Therefore, according to the above parameters, the migration energy in the experiment is approximately calculated as 1.75 eV.

In addition, with regards to our calculations, as can be seen from Table 2, the migration energy of N_i with -1 charge state is 1.80 eV, which is in good agreement with the experimental results and closer than other works [18,19]. In other words, this comparable result provides another perspective to prove our results.

4. Conclusions

In the present work, ab initio calculations have been performed to investigate the defect of nitrogen interstitial (N_i) in GaN material. With regards to different N_i configurations, it is found that the most stable configuration of N_i presents a threefold symmetry in each layer and different charge states of N_i show a similar orientation but different bond lengths.

For the nearest in-plane migration of N_i , a rotation process which has not been reported is observed. Due to this process, the in-plane migration is found to be divided into two paths, upward and downward paths and the migration barriers of them differ at some charge states. Different from previous studies, our specific work shows that the migration of N atom is an anisotropic process, especially in the migration mechanisms. Furthermore, part of our results of migration of N_i are consistent well with the existing experiments and the corresponding theories.

As for charged N Frenkel pair, it is found to be a relatively stable defect complex as expected. According to the results of bond length and charge analysis, the charged complex $(N_i-V_N)^q$ may consist of $(N_i)^{q-1}$ and $(V_N)^{+1}$. Additionally, the calculations of binding energy and recombination barrier also reveal that the well separation distance of N_i-V_N is about 3.9 Å.

The calculated results are useful to reveal some mechanisms of point defect in GaN, i.e., rotation behavior and charged Frenkel pair. This work also provides helpful perspectives in the identification and dynamics studies of GaN material by a theoretical sight.

Supplementary Materials: The following are available online at <http://www.mdpi.com/1996-1944/13/16/3627/s1>. Figure S1: Direct migration; Figure S2: Indirect migration.

Author Contributions: Conceptualization: C.H. W.L. (Wenbo Liu) and H.Z. (Hang Zang); methodology: H.H., P.Z., D.T., and L.Y.; formal analysis: H.H., W.L. (Wenlong Liao) and H.Z. (Hongxiang Zong); funding: C.H., H.Z. (Hang Zang), and W.L. (Wenbo Liu); writing: H.H.; review and editing: P.Z., W.L. (Wenbo Liu), C.H., and H.Z. (Hongxiang Zong). All authors have read and agreed to the published version of the manuscript.

Funding: The research was supported by the Science Challenge Project (No. TZ2018004) and the National Natural Science Foundation of China (Grant No. 11835006, 11775167, 11690040, and 11690043).

Conflicts of Interest: The authors declare no conflict of interest.

Appendix A

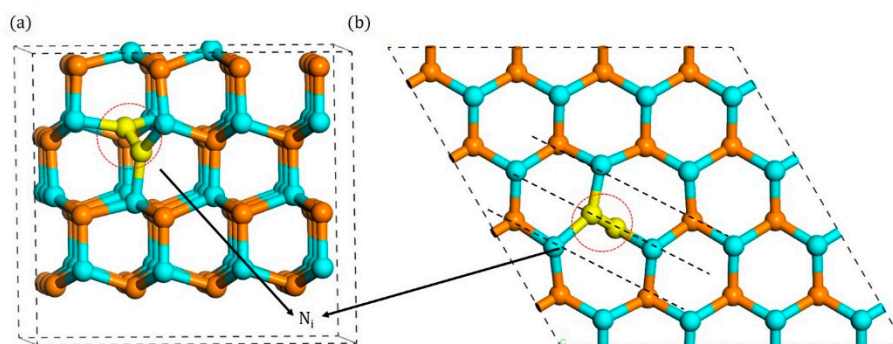


Figure A1. Configurations of B_1 type split interstitial: (a) side view and (b) top view.

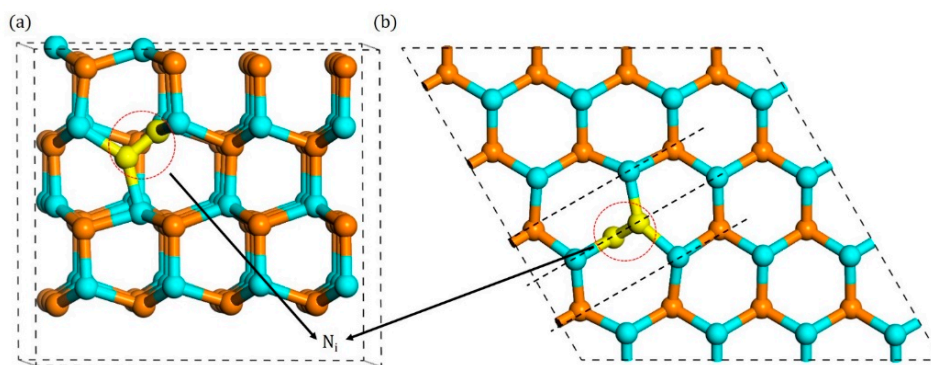


Figure A2. Configurations of B₂ type split interstitial: (a) side view and (b) top view.

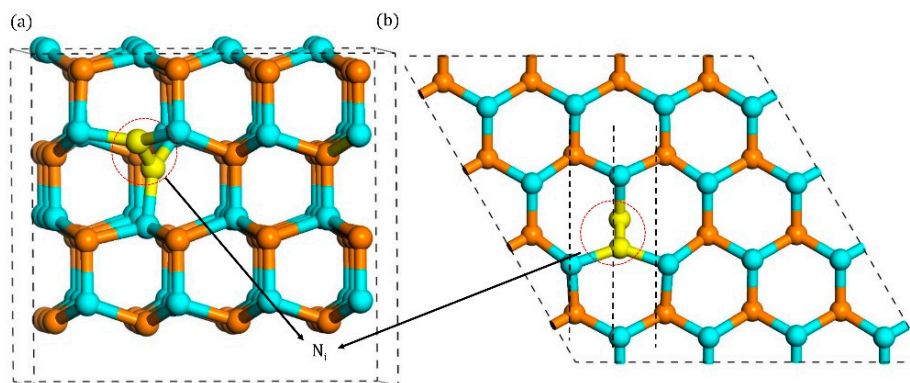


Figure A3. Configurations of B₃ type split interstitial: (a) side view and (b) top view.

References

1. Li, Y.-C.; Chang, L.-B.; Chen, H.-J.; Yen, C.-Y.; Pan, K.-W.; Huang, B.-R.; Kuo, W.-Y.; Chow, L.; Zhou, D.; Popko, E. Phosphor-Free InGaN White Light Emitting Diodes Using Flip-Chip Technology. *Materials* **2017**, *10*, 432. [[CrossRef](#)] [[PubMed](#)]
2. Polyakov, A.Y.; Lee, I.-H. Deep traps in GaN-based structures as affecting the performance of GaN devices. *Mater. Sci. Eng. R Rep.* **2015**, *94*, 1–56. [[CrossRef](#)]
3. Nguyen, H.T.; Yamada, H.; Yamada, T.; Takahashi, T.; Shimizu, M. Fabrication and Evaluation of N-Channel GaN Metal–Oxide–Semiconductor Field-Effect Transistors Based on Regrown and Implantation Methods. *Materials* **2020**, *13*, 899. [[CrossRef](#)] [[PubMed](#)]
4. He, H.; He, C.; Zhang, J.; Liao, W.; Zang, H.; Li, Y.; Liu, W.-B. Primary damage of 10 keV Ga PKA in bulk GaN material under different temperatures. *Nucl. Eng. Technol.* **2020**, *52*, 1537–1544. [[CrossRef](#)]
5. Weaver, B.D.; Martin, P.A.; Boos, J.B.; Cress, C.D. Displacement Damage Effects in AlGaIn/GaN High Electron Mobility Transistors. *IEEE Trans. Nucl. Sci.* **2012**, *59*, 3077–3080. [[CrossRef](#)]
6. Costanzo, F.; Giofre, R.; Massari, A.; Feudale, M.; Suriani, A.; Limiti, E. A MMIC power amplifier in GaN on Si technology for next generation Q band high throughput satellite systems. *Integration* **2019**, *68*, 139–146. [[CrossRef](#)]
7. Belabbas, I.; Chen, J.; Nouet, G. Electronic structure and metallization effects at threading dislocation cores in GaN. *Comput. Mater. Sci.* **2014**, *90*, 71–81. [[CrossRef](#)]
8. Ene, V.L.; Dinescu, D.; Zai, I.; Djourellov, N.; Vasile, B.S.; Serban, A.B.; Leca, V.; Andronescu, E. Study of Edge and Screw Dislocation Density in GaN/Al₂O₃ Heterostructure. *Materials* **2019**, *12*, 42055. [[CrossRef](#)]
9. Kanegae, K.; Fujikura, H.; Otoki, Y.; Konno, T.; Yoshida, T.; Horita, M.; Kimoto, T.; Suda, J. Deep-level transient spectroscopy studies of electron and hole traps in n-type GaN homoepitaxial layers grown by quartz-free hydride-vapor-phase epitaxy. *Appl. Phys. Lett.* **2019**, *115*, 012103. [[CrossRef](#)]

10. Sunay, U.R.; E Zvanut, M.; Marbey, J.; Hill, S.; Leach, J.H.; Uduary, K. Small non-uniform basal crystal fields in HVPE free-standing GaN:Mg as evidenced by angular dependent and frequency-dependent EPR. *J. Phys. Condens. Matter*. **2019**, *31*, 345702. [[CrossRef](#)]
11. Van Bardeleben, H.J.; Cantin, J.-L.; Gerstmann, U.; Scholle, A.; Greulich-Weber, S.; Rauls, E.; Landmann, M.; Schmidt, W.G.; Gentils, A.; Botsoa, J.; et al. Identification of the Nitrogen Split Interstitial (N-N)_N in GaN. *Phys. Rev. Lett.* **2012**, *109*, 206402. [[CrossRef](#)] [[PubMed](#)]
12. Gao, F.; Bylaska, E.J.; Weber, W.J. Intrinsic Defect Properties in GaN Calculated by Ab Initio and Empirical Potential Methods. *Phys. Rev. B* **2004**, *70*, 245208. [[CrossRef](#)]
13. Lyons, J.L.; Van de Walle, C.G. Computationally predicted energies and properties of defects in GaN. *NPJ Comput. Mater.* **2017**, *3*, 180. [[CrossRef](#)]
14. Gao, Y.; Sun, D.; Jiang, X.; Zhao, J. Point defects in group III nitrides: A comparative first-principles study. *J. Appl. Phys.* **2019**, *125*, 215705. [[CrossRef](#)]
15. Matsubara, M.; Bellotti, E. A first-principles study of carbon-related energy levels in GaN: I. Complexes formed by substitutional/interstitial carbons and gallium/nitrogen vacancies. *J. Appl. Phys.* **2017**, *121*, 195701. [[CrossRef](#)]
16. Xie, Z.; Sui, Y.; Buckeridge, J.; A Catlow, C.R.; Keal, T.W.; Sherwood, P.; Walsh, A.; Farrow, M.R.; Scanlon, D.O.; Woodley, S.M.; et al. Donor and acceptor characteristics of native point defects in GaN. *J. Phys. D Appl. Phys.* **2019**, *52*, 335104. [[CrossRef](#)]
17. Diallo, I.C.; Demchenko, D.O. Native Point Defects in GaN: A Hybrid-Functional Study. *Phys. Rev. Appl.* **2016**, *6*, 064002. [[CrossRef](#)]
18. Kyrtsos, A.; Matsubara, M.; Bellotti, E. Migration mechanisms and diffusion barriers of carbon and native point defects in GaN. *Phys. Rev. B* **2016**, *93*, 245201. [[CrossRef](#)]
19. Limpijumnong, S.; Van de Walle, C.G. Diffusivity of native defects in GaN. *Phys. Rev. B* **2004**, *69*, 035207. [[CrossRef](#)]
20. Kresse, G.; Furthmüller, J. Efficient iterative schemes for ab initio total-energy calculations using a plane-wave basis set. *Phys. Rev. B* **1996**, *54*, 11169–11186. [[CrossRef](#)]
21. Perdew, J.P.; Burke, K.; Ernzerhof, M. Generalized Gradient Approximation Made Simple. *Phys. Rev. Lett.* **1996**, *77*, 3865–3868. [[CrossRef](#)] [[PubMed](#)]
22. Kresse, G.; Joubert, D. From ultrasoft pseudopotentials to the projector augmented-wave method. *Phys. Rev. B* **1999**, *59*, 1758–1775. [[CrossRef](#)]
23. Henkelman, G.; Uberuaga, B.P.; Jónsson, H. A climbing image nudged elastic band method for finding saddle points and minimum energy paths. *J. Chem. Phys.* **2000**, *113*, 9901–9904. [[CrossRef](#)]
24. Henkelman, G.; Jónsson, H. A dimer method for finding saddle points on high dimensional potential surfaces using only first derivatives. *J. Chem. Phys.* **1999**, *111*, 7010–7022. [[CrossRef](#)]
25. Jain, A.; Ong, S.P.; Hautier, G.; Chen, W.; Richards, W.D.; Dacek, S.; Cholia, S.; Gunter, D.; Skinner, D.; Ceder, G.; et al. Commentary: The Materials Project: A materials genome approach to accelerating materials innovation. *APL Mater.* **2013**, *1*, 11002. [[CrossRef](#)]
26. Schulz, H.; Thiemann, K. Crystal structure refinement of AlN and GaN. *Solid State Commun.* **1977**, *23*, 815–819. [[CrossRef](#)]
27. Freysoldt, C.; Neugebauer, J.; Van De Walle, C.G. Fully Ab Initio Finite-Size Corrections for Charged-Defect Supercell Calculations. *Phys. Rev. Lett.* **2009**, *102*, 016402. [[CrossRef](#)]
28. Chung, J.W.; Hoke, W.; Chumbes, E.; Palacios, T. AlGaIn/GaN Hemt with 300-GHz Fmax. *IEEE Electron. Device Lett.* **2010**, *31*, 195–197. [[CrossRef](#)]
29. Weichuan, X.; Liu, Z.; Qiu, H.; Ranjan, K.; Palacios, T. InAlN/GaN Hemts on Si with High f_T of 250 GHz. *IEEE Electron. Device Lett.* **2017**, *39*, 75–78.
30. Tang, W.; Sanville, E.; Henkelman, G. A grid-based Bader analysis algorithm without lattice bias. *J. Phys. Condens. Matter* **2009**, *21*, 084204. [[CrossRef](#)]
31. Henkelman, G.; Arnaldsson, A.; Jónsson, H. A fast and robust algorithm for Bader decomposition of charge density. *Comput. Mater. Sci.* **2006**, *36*, 354–360. [[CrossRef](#)]
32. Beck, M.J.; Tsetseris, L.; Pantelides, S.T. Stability and Dynamics of Frenkel Pairs in Si. *Phys. Rev. Lett.* **2007**, *99*, 215503. [[CrossRef](#)] [[PubMed](#)]
33. Dippong, T.; Levei, E.A.; Cadar, O.; Goga, F.; Toloman, D.; Borodi, G. Thermal behavior of Ni, Co and Fe succinates embedded in silica matrix. *J. Therm. Anal. Calorim.* **2019**, *136*, 1587–1596. [[CrossRef](#)]

34. Gerstmann, U.; Rauls, E.; Frauenheim, T.; Overhof, H. Formation and annealing of nitrogen-related complexes in SiC. *Phys. Rev. B* **2003**, *67*, 205202. [[CrossRef](#)]
35. Sahoo, B.K.; Sahoo, S.K.; Sahoo, S. Macroscopic polarization and thermal conductivity of GaN. *J. Phys. Chem. Solids* **2013**, *74*, 1669–1671. [[CrossRef](#)]



© 2020 by the authors. Licensee MDPI, Basel, Switzerland. This article is an open access article distributed under the terms and conditions of the Creative Commons Attribution (CC BY) license (<http://creativecommons.org/licenses/by/4.0/>).